Information Sciences Letters

Volume 11
Issue 2 *Mar. 2022*

Article 47

2022

Study of Optical, Electrical and Photocatalysis Properties of SrMnO3 Synthesized by Solid-State Reaction

Mahrous R. Ahmed
Physics Department, Faculty of Science, Sohag University, Sohag 82524, Egypt,
ahmedhakeem75@yahoo.com

H. M. Ali
Physics Department, Faculty of Science, Sohag University, Sohag 82524, Egypt,
ahmedhakeem75@yahoo.com

M. F. Hasaneen
Physics Department, Faculty of Science, Sohag University, Sohag 82524, Egypt\\ Physics Department, College of Science, Jouf University, Al-Jouf, P.O. Box 2014, Sakaka, Saudi Arabia,
ahmedhakeem75@yahoo.com

Amira Etman
Physics Department, Faculty of Science, Sohag University, Sohag 82524, Egypt,
ahmedhakeem75@yahoo.com

Information Sciences Letters
An International Journal

http://dx.doi.org/10.18576/isl/110216

Study of Optical, Electrical and Photocatalysis Properties of $SrMnO_3$ Synthesized by Solid-State Reaction

Mahrous R. Ahmed[1], *H. M. Ali*[1], *M. F. Hasaneen*[1,2] , *Amira Etman*[1] *and A. M. Abdel hakeem*[1,*]

[1]Physics Department, Faculty of Science, Sohag University, Sohag 82524, Egypt
[2]Physics Department, College of Science, Jouf University, Al-Jouf, P.O. Box 2014, Sakaka, Saudi Arabia

Received: 21 Dec. 2021, Revised: 15 Jan. 2022, Accepted:25 Jan. 2022.
Published online:1 Mar. 2022.

Abstract: $SrMnO_3$ was prepared by solid-state reaction method to obtain powder then thin films by a thermal evaporation method. XRD diffraction, Optical and electrical properties were investigated. Photocatalysis process was implemented as an interesting application of $SrMnO_3$. XRD diffraction results were used to study the compound structure and to calculate some other parameters such as crystallite size, D, microstrain, ε, and dislocation density, δ. XRD results revealed that $SrMnO_3$ has a polycrystalline structure such as hexagonal structure for $SrMnO_3$ phase and tetragonal structure for MnO_2 phase. The optical energy band for the powder and thin film were equal to 2.28 eV and 2.92 eV respectively, which candidates this compound to be a solar cell transparent window, especially for deposited thin films. The electrical resistivity behaved as semiconductor-like where it decreases with the temperature with electrical activation energy equal 0.960 eV when heating and 0.663 eV when cooling. The result of the Methylene blue absorption showed that the $SrMnO_3$ powder does work very well as a Photocatalyst. The efficiency of the powder of $SrMnO_3$ as a Photocatalyst increases with the illumination time and its best value is about 56% at 120 min.

Keywords: $SrMnO_3$, X-ray, Reflectance, Transmittance, Photocatalysis**,** resistivity.

1 Introduction

Metal oxides are very important compounds for applications in the field of science and technology which were studied experimentally and theoretically [1,2,3,4,5,6,7]. It depends on their electrical and optical energy gap. Some Metal oxides are semiconductors which have medium energy gap while others are considered insulators because of their high energy gap. Optically, the metal oxides compounds which have about a 3.5 eV energy gap are considered visible absorption. If impurities or dopants are added to the metal oxides they can have color.

Alok Tiwari et al [8] have analyzed experimentally and theoretically the syntheses of SrMnO3 thin films prepared using pulsed lased deposition method. They obtained that XRD diffraction showed that SrMnO3 thin film has an orthorhombic phase structure.

Dung et. al. [9] studied the effect of the random incorporation of $SrMnO_3$ into the structure of Bi0.5Na0.5TiO3. They obtained a distortion in the lattice and a reduction in the optical energy gap from 3.07 eV to 1.81 eV. While Sousan and Niasari [10] have used many methods to prepare nanoparticles of $SrMnO_3$ and measured the optical properties for the powder of this compound. They estimated a value of the optical energy gap of the powder as = 4.3 eV. The optical energy gap increased compared to the bulk structure of the same compound. They attributed that to the decreasing of the size of the grains of the powder.

Gang et al [11] have studied the electronics and optical properties of rare-earth manganite compounds theoretically. Optical properties of such compounds such as the reflectance were studied. They obtained one peak working at 3.6 eV in the reflectance dispersion of their compound which leads to a leaner proportion with increasing the dopant.

$SrMnO_3$ had few works done and not been covered by enough researches to study its promising electrical, optical properties and the applications such as Photocatalysis, solar cells and electronic devices. In this work, we investigated the electrical and optical properties of SrMnO3 and the possibility of using this compound as a Photocatalyst for organic impurities. Experimental techniques are explained in section 2, while the results and discussion are shown in section 3. We conclude our results in section 4.

*Corresponding author e-mail: ahmedhakeem75@yahoo.com

2 Experimental Techniques

2.1 Powder Preparation

Stoichiometry of 99.99% purity of both SrO and MnO were secured by Sigma-Aldrich. The powder from $SrMnO_3$ compound was prepared by solid-state reaction method. The required quantity of the compound was prepared after mixing the elements in proportions depending on the sample weight and the atomic weights. The compound was ground for 12 hours. Then the sintering of the ground compound was carried out for 5 hours in an oven at 650°C. The grinding process was resumed for another 3 hours to obtain a well-ground powder sample with nano-grains size.

2.2 Thin Film Preparation

A part of the prepared powder was taken to deposit the needed thin films using thermal vacuum evaporation unit (Edward's model; AUTO 306). Thin films were deposited with 100 nm thickness on substrates from glass under pressure 10^{-5} bar.

2.3 Photocatalysis

The photocatalysis process, as an application of our composition $SrMnO_3$ in purification of the contaminated organic solutions, has been implemented for the powder as follows: Methylene blue, MB, the solution was prepared where 0.001 grams of blue dye is added to 100 milliliters of distilled water. The absorption measurement is carried out for the Methylene blue solution, then, we added 0.5 gm of the powder in the solution and left that mixture in the dark for one hour, after that we measured the absorption another time. Finally, the solution is exposed to ultraviolet illumination source for 5, 10, 15, 20 .... and 120 minutes with measuring the absorption for the solution each time.

The Photocatalysis process has been implemented for the thin film deposited on a glass substrate as follows: A portion of the previously prepared the Methylene blue the solution was taken to study possibility of using our thin films in purification of the contaminated organic solutions. The absorption measurement is carried out for the Methylene blue solution, then, we added thin film in the solution and left that mixture in the dark for one hour, then we measured the absorption another time. Finally, the solution is exposed to an ultraviolet source for 5, 10, 15, 20 .... and 120 minutes with measuring the absorption for the solution every time.

2.4 Optical Measurement

Some optical measurements, such as transmittance, T, reflectance, R, and absorbance, A, and some optical parameters such as refractive index, n, absorption coefficient, α, and extinction coefficient, K, were investigated using the spectrophotometer device model (JASCO, V-570) with UV–vis–near-infrared and some calculations. Optical measurements were done into a wavelength range from 400 nm to 2500 nm.

2.5 Electrical Properties

The electrical properties were measured for our thin films to compare the optical energy gap with the electrical energy gap and study the behavior of the electrical resistivity and the transition temperature using the electrode-electrode method. Two electrodes were fixed on the film terminals with silver paste. Electric field with microvolt range was applied and the voltage and current were measured using micrometers devices.

2.6 XRD Diffraction

The crystal structure phases of our powder and thin films samples were investigated using X-ray diffraction model ((Philips X'pert MRD) with Cu-Ka radiation (i.e., λ = 1.5418 A), incident angle of 0.75◦ and over a 2θ scan range between 10° and 80°.

3 Results and Discussion

3.1 Structural Analyses by XRD

Figure (1) shows XRD spectrum of $SrMnO_3$ thin film deposited on glass substrate and sintering at 650°C. The dominant peaks relating to $SrMnO_3$ phase have a hexagonal structure (JCPDS card no. 24-1213). Second phase that is related to MnO_2 phase (JCPDS card no. 043-1031) has a tetragonal shape is observed. There is great competition between $SrMnO_3$ phase formation and the MnO_2 impurity phase. The effect of oxide impurity phase is studied, in nanoscale [12], on the optical properties of $SrMnO_3$ phase.

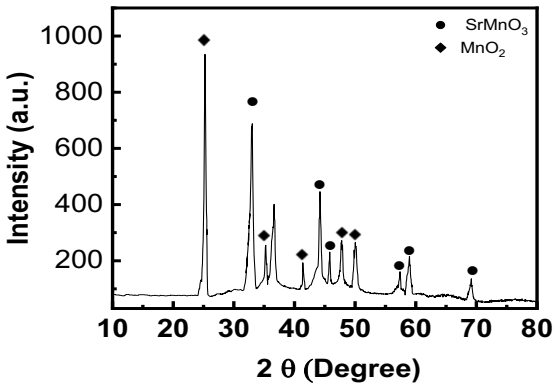

Fig.1: XRD pattern of $SrMnO_3$ thin film deposited on glass substrate and sintered at 650°C.

Figure (1) shows XRD spectrum of $SrMnO_3$ thin film deposited on glass substrate and sintering at 650°C. The dominant peaks relating to SrMnO3 phase have a hexagonal structure (JCPDS card no. 24-1213). Second phase that is related to MnO2 phase (JCPDS card no. 043-

1031) has a tetragonal shape is observed. There is great competition between SrMnO3 phase formation and the MnO2 impurity phase. The effect of oxide impurity phase is studied, in nanoscale, on the optical properties of SrMnO3 phase.

To calculate the crystal size, D, Debye-Scherrer equation is used [13]:

$$D = \frac{0.9\,\lambda}{\beta \cos\theta} \quad (1)$$

Where β is the line broadening at the full width of the half maximum (FWHM), θ is the Bragg angle, and λ is the X-ray wavelength of 1.541 Å. The average crystal size is found lower than 30 nm for all the oxide impurity phases obtained from this compound by XRD pattern.

The internal microstrains, ε, are existed in the compressed powder sample due to different stresses applied to the structure. The internal microstrain can be calculated according to the following equation [14]

$$\varepsilon = \beta\cos\theta/4\sin\theta \quad (2)$$

The microstrain at the contact points among crystal grains can extend to a very wide range and, as a result, the diffraction peaks broaden significantly as depicted in table (1).

The number of defects in the crystal can be measured by the dislocation density, δ, which is defined as the length of dislocation lines per unit volume. It can be calculated from the following relation [14]:

$$\delta = D^{-2} \quad (3)$$

The dislocation density varies in the range between 3.369×10^{-3} at 2θ = 58.96° and 7.288×10^{-3} at 2θ = 33.04°. This variation is because the defects formation centers depend on the crystal size, D, in a nanoscale (lower than 30 nm) as shown in table (1).

Table 1: Crystallite size, D, microstrain, ε, and dislocation density, δ, of $SrMnO_3$ thin film deposited on glass substrate and sintered at 650°C for 5 hours.

The name of phase	2θ (°)	FWHM	D (nm)	microStrain (ε) ($*10^{-3}$ nm^{-2})	Dislocation energy (δ) ($*10^{-3}$)
MnO_2	25.24	0.42577	19.14	2.7281	8.079
$SrMnO_3$	33.04	0.49544	16.72	3.5748	7.288
$SrMnO_3$	35.26	0.3285	25.37	1.5530	4.510
MnO_2	41.38	0.58558	14.29	4.8967	6.29
$SrMnO_3$	44.2	0.36481	23.50	1.8102	3.592
$SrMnO_3$	46.35	0.36481	23.50	1.8102	3.592
MnO_2	47.79	0.3942	22.04	2.0582	3.686
MnO_2	50.12	0.55137	15.89	3.9560	4.255
$SrMnO_3$	58.96	0.43652	20.90	2.2880	3.369
$SrMnO_3$	69.16	0.6047	15.95	3.9275	3.827

3.2 Optical Measurements

The optical properties of our composition $SrMnO_3$ in forms of both thin films and powder are investigated by measuring the transmittance, T, reflectance, R and absorption, A, and calculating the refractive index, n, extinction coefficient, K, absorption coefficient, α, and optical energy gap, E_g.

3.2.1The Transmittance and Reflectance Dispersion

The transmittance, T, and reflectance, R, are measured as a function of a range wavelength from 400 nm to 2500 nm using UV–vis–near-infrared spectrophotometer for the thin film sample deposited on a glass substrate. While the reflectance, R, is measured by the same method for the powder sample.

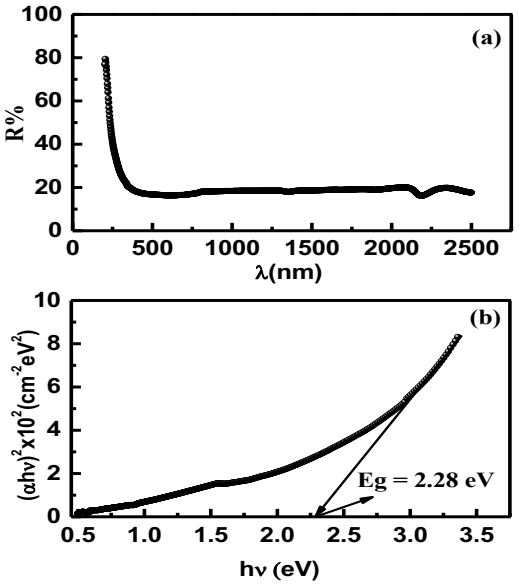

Fig. 2: **a**) The reflectance, R, as function of the wavelength. **b**) Tauc's equation to determine the optical energy gap, E_g. Both figures are for the powder sample of $SrMnO_3$.

The optical band gap of powder material is achieved by measuring the light diffused reflection by UV-VIS spectroscopy (UV-Vis DR). The Kubelka-Munk method [15,16] is used to estimate the optical energy gap, E_g, for the powder materials with all doping, x, values as follows:

$$F(R) = \frac{\alpha}{S} = \frac{(1-R)^2}{2R} \quad (4)$$

where F(R) is the Kubelka-Munk function, α is the absorption coefficient, S is the scattering coefficient and R is the reflectance. Extrapolating the straight line portion of the curve in the energy axis of the relation between $[F(R)h\nu]^n$ and the photon energy, hν, estimates the values of band gap energy, Eg.. The factor n is representing the direct or indirect allowed and forbidden electronic transition respectively. Here, n equals 1/2 which means that the transition is direct [10]. Fig. (2) b shows the relation between the linear part of $(\alpha h\nu)^2$ as a function of $(h\nu)$ at α=0. After the extrapolation of the linear part, E_g is obtained to equal 2.28 eV which is comparable with the result obtained in ref. [10].

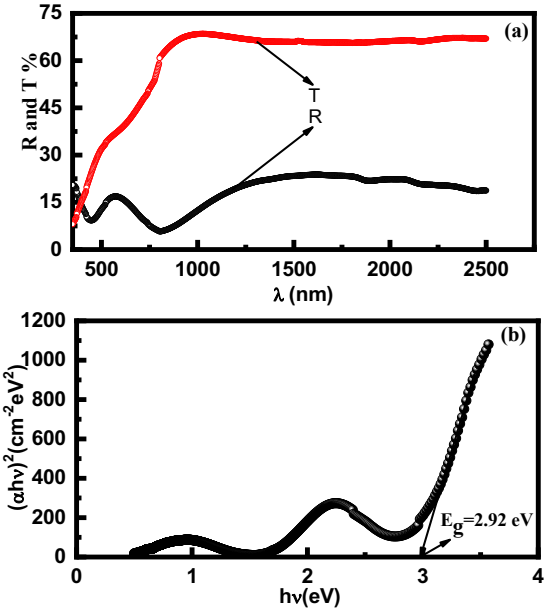

Fig. 3: **a)** Reflectance, R, and Transmittance, T, as function of the wavelength, λ. **b)** Tauc's equationis used to determine the optical energy gap, E_g. Both figures are for $SrMnO_3$ thin films sample deposited on glass substrate

It is found from Fig. (3) a for the thin film deposited on glass substrate that the reflectance, R, obtains its minimum value at a wavelength equal to 802 nm, while the transmittance, T, reaches its maximum value at a wavelength equal to 1000 nm. The maximum intensity of the reflectance is close to 40% which is located at the beginning of the range of the visible region. The difference between R and T is nearly equal to the absorption, A, where R+T+A=100%. The optical activation energy, E_g, for that film is calculated from the linear part shown in Fig. (3) b using Tauc's equation (4). E_g is found equal 2.92 eV for the deposited film on glass substrate. This result agree very well with the published results [17]. In addition, these results of E_g make this compound a candidate to be used as a window layer in solar cell applications.

3.2.2 Calculation of Some of the Optical Parameters

Fig. (4) a, b and c show the dependence of the refractive index, absorption coefficient, α, and the extinction coefficient, k, on the wavelength, λ, respectively, for the $SrMnO_3$ thin film deposited on glass substrate.
The refractive index, shown in Fig (4)a as a function of the wavelength is calculated from the following equation [18,19]

$$n = \frac{1+R^{0.5}}{1-R^{0.5}} \qquad (5)$$

Where R is the reflectance. It decreases fluctuatingly with increasing of λ till reaches 1.63 when λ=802 nm, then it increases slowly till it reaches 2.9 at λ = 1600 nm. Finally, n decreases again very slowly to get 2.5 value at the end of λ range. The refractive index has relatively low values where that means our thin film has somewhat low density.

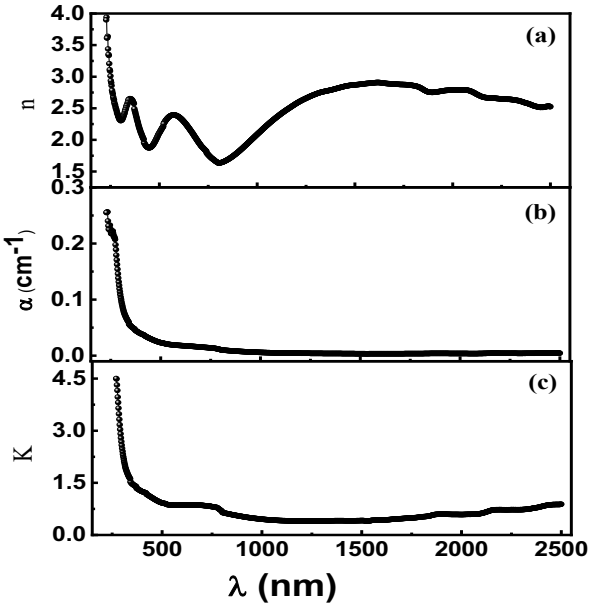

Fig.4: The dependence of the refractive index, n, **a)**, absorption coefficient, α, **b)**, and the extinction coefficient, k, **c)** on the wavelength, λ, for the $SrMnO_3$ thin film deposited on glass substrate.

Absorption coefficient, α, is shown in Fig. (4) b. α could be calculated from the following equation [20,21,22],

$$\alpha = \frac{2.303}{d} Ln(\frac{1-R}{T}) \qquad (6)$$

Where T is the transmittance and *d* is the film thickness. Absorption coefficient, α, frankly decreases promptly with increasing of the wavelength until λ =1000 nm, then α is going to be stable up till the end of the wavelength range. The results of α are compatible with the results of R and T shown in Fig. (3) a where at the point of the maximum of T and the minimum of R, namely =1000 nm, the absorption coefficient of our thin film has its minimum value too. It means that the film tends to be a good transparent at UV range that makes it a candidate to be used as a transparent window in solar cell applications.
The extinction coefficient, K, is given by this equation [19,20]:

$$K = \frac{\alpha\lambda}{4\pi} \qquad (7)$$

Fig. (4) c reveals the relation between the extinction coefficient, K, and the wavelength, λ. The extinction coefficient means how the thin film absorbs the light at the whole range of the wavelength. As seen from the figure that K decreases dramatically when λ increases, then, after λ=800 nm, K begins to be stable to the end of λ range. It

seems that the visible region is the most effective range which influences on the behavior of K and α.

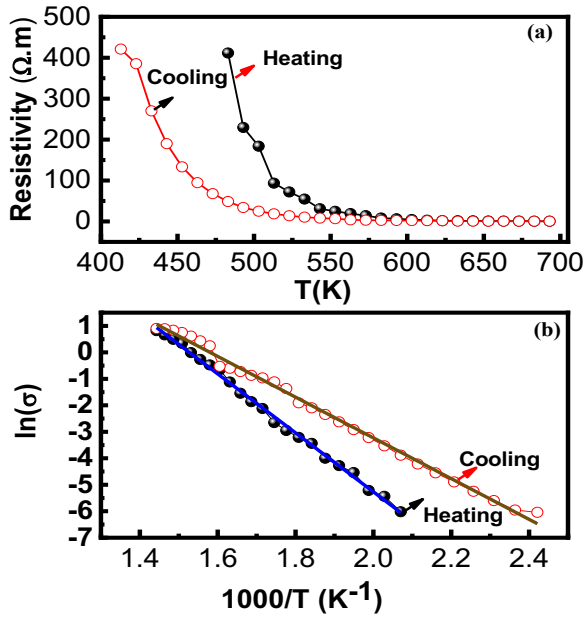

Fig.5: a): the temperature dependence of the electrical resistivity during heating and cooling process. **b)** The logarithm of the conductivity, Ln(σ), as a function of 1000/T. Both figures are for the film sample deposited on glass substrate.

3.3 The Electrical Properties

The electrical behavior of the thin film deposited on a glass substrate is very important to compare it with the optical parameters and to help us to interpret the results in light of the electronic structure. The behavior of the film resistivity, ρ, with absolute temperature, T(K), is shown in Fig. (5). It is noticed that the resistivity decreases exponentially starting with a value above 420 Ω.m for both heating and cooling direction.

Frankly, the film behaves as semiconductor-like with the temperature increasing. In addition, it is clear from the figure that the resistivity has different values at heating from cooling where its values when heating is higher than that when cooling. That can be attributed to the hopping between Mn3+ and Mn4+ ions [23] caused by the different oxides phases that appeared in the structure by XRD. The relation between the logarithm of the conductivity, Ln(σ), as a function of 1000/T is fitted to estimate the electrical activation energy, E_{eg}, as shown in Fig. (5) b. It is found to be equal to 0.960 eV when heating and 0.663 eV when cooling which is close to the values in ref. [24].

3.4 Photocatalysis Process

One of the biggest industrial challenges is to find a cheap and environmental friendly catalyst for water splitting. Manganese is one of the most candidate elements [25] to be used in water splitting because of its cheap and green effect on the environment. Its compounds are known as the natural catalysts used by plants and algae for water oxidation [26,27,28]. The oxidation of water is an interesting effect of the photocatalysts such as $SrMnO_3$ compound.

We use our SrMnO3 compound in both powder and thin film deposited on a glass substrate as Photocatalyst in order to purify the impure water from organic contamination such as Methylene blue (MB). MB solution which was prepared as mentioned above is used as organically impure water. We follow the procedures mentioned in section 2.3 to obtain the results of using our compound as a Photocatalyst.

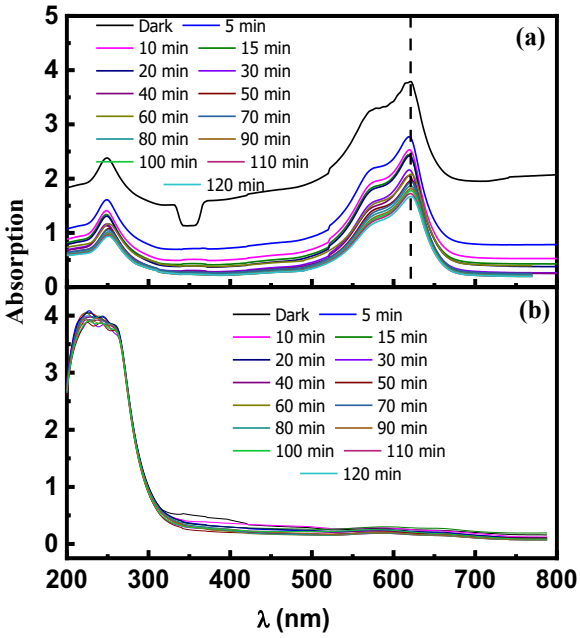

Fig.6: a) The absorption measurement for the powder Photocatalyst application. **b)** The absorption measurement for the thin film deposited on glass substrate Photocatalyst application. Both figures **a)** and **b)** as a function of wavelength before and after illumination by UV light.

Fig. (6) a and b show the variation of the absorption spectra of the Methylene blue (MB) before and after exposure the solution to UV illumination, for the powder in Fig. (6) a and for the thin film deposited on glass substrate in Fig. (6) b. It is worth mentioning that the effect of the UV illumination time on the MB mixed with the powder is clear and reveals the role of the powder of $SrMnO_3$ compound as Photocatalyst for water purification as seen from Fig. (6) a. The absorption, A, decreases with increasing the UV illumination time and it has its maximum at wavelength equals to 620 nm which means that the solution transparency increases with increasing UV illumination time. While the effect of the UV illumination time on the MB when the film is dipped is not clear, so thin films of this compound are not suitable to work as Photocatalyst.

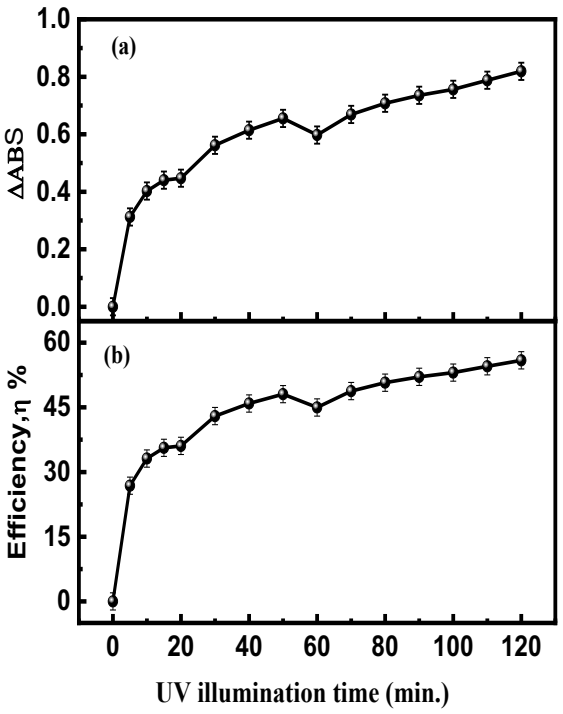

Fig.7: The degradation **a)** and The efficiency **b)** of the $SrMnO_3$ powder as Photocatalyst for water purification as a function of UV illumination time at 620 nm.

It is noticed from Fig. (7) a that the absorption maximum value increases with increasing of the time of UV illumination from 5 min. to 50 min.. After 50 min the degradation increases slowly till the absorption reaches 80% at 120 min. Fig. (7) b shows that the efficiency of the powder of $SrMnO_3$ as a Photocatalyst increases with the illumination time and its best value is about 56% at 120min. That is interpreted as the increase of the UV illumination motivates the powder grains to interact with MB grains and make them precipitate in the bottom of the container, or the powder grains decompose the MB suspended grains with increasing the time of the UV illumination.

4 Conclusions

One concludes the results of this work as follows; A powder was prepared by the solid-state interaction method and sintered for 12 hours at 650ºC. Thin films were deposited by the thermal evaporation method on a glass substrate. XRD results revealed that $SrMnO_3$ phase with hexagonal structure and second phase of MnO_2 with tetragonal structure have been obtained. Also, Crystallite size (D), microstrain, ε, and dislocation density, δ, were calculated.

The optical properties of our compound in both powder and thin film have been investigated. It was found that the thin film could be a candidate to work as a transparent window in the solar cells structure. This result was supported by finding the optical energy band of the thin film is 2.92 eV which candidates this $SrMnO_3$ thin film to be a solar cell transparent window. The dependence of the refractive index, n, absorption coefficient, α, and the extinction coefficient, K, on the wavelength, λ, were calculated for the $SrMnO_3$ thin film deposited on a glass substrate.

The electrical resistivity of $SrMnO_3$ film was investigated when heating and cooling. The film showed semiconductor-like behavior for both directions. The electrical activation energy were equal 0.960 eV when heating and 0.663 eV when cooling. This was attributed to the change in the hopping occurring between Mn^{+3} and Mn^{+4} ions in $SrMnO_3$.

We used both $SrMnO_3$ compound powder and thin film deposited on a glass substrate as a Photocatalyst in order to purify the impure water from organic contamination. The results showed that the powder is much better as Photocatalyst than the thin film deposited on a glass substrate. The efficiency of the powder of $SrMnO_3$ as a Photocatalyst increases with the illumination time and its best value is about 56% at 120min. That was interpreted as the increase of the UV illumination motivating the powder grains to interact with MB grains and make them precipitate in the bottom of the container, or the powder grains decompose the MB suspended grains with increasing the time of the UV illumination. The result of the Methylene blue absorption tells us that the $SrMnO_3$ powder does work very well as a Photocatalyst.

Conflicts of Interest

The authors declare that there is no conflict of interest regarding the publication of this article.

References

[1] T. W Noh., J. H. Jung, H. J. Lee, K. H. Kim, J. Yu, E. Choi, Optical Properties of Perovskite Manganites. J. and Moritomo Y., Journal of the Korean Physical Society, 36, 392-397 (2000).

[2] W. Xia, H. Wu, P. Xue and X. Zhu, Microstructural, magnetic, and optical properties of Pr-doped perovskite manganite La0. 67Ca0. 33MnO3 nanoparticles synthesized via sol-gel process. Nanoscale Research Letters, 13:135 (2018).

[3] J. Bai, J. Yang, W. Dong, Y. Zhang, W. Bai, X. Tang, Structural and magnetic properties of perovskite SrMnO3 thin films grown by molecular beam epitaxy. Thin Solid Films, 644, 57-64 (2017).

[4] Yu. P. Sukhorukov, E. A. Gan'shina, A. R. Kaul, O. Yu. Gorbenko, N. N. Loshkareva, A. V. Telegin, M. S. Kartavtseva, and A. N. Vinogradov, $Sm_{0.55}Sr_{0.45}MnO_3$ / $Nd_{0.}$

$_{55}Sr_{0.45}MnO_3$ heteroepitaxial structure: Optical and magnetotransport propertiesTechnical Physics, 53, 716-721 (2008).

[5] A. M. Aliev, A. B. Batdalov, and L. N. Khanov, Magnetic and lattice contributions to the magnetocaloric effect in Sm1-xSrxMnO3 manganites. Appl. Phys. Lett, 112, 142407 (2018).

[6] I. A. Abdel-Latif, M. R. Ahmed, I. A. Al-Omari, A. Sellai, Journal of Magnetism and Magnetic Materials, 420, 363–370 (2018).

[7] M. R. Ahmed, Monte Carlo study of the effect of charge ordering on the electrical and magnetic properties of half-doped manganites. Journal of Magnetism and Magnetic Materials, 504, 166628 (2020).

[8] A. Tiwari, B. Pandey, R. Mishra, A. V. Rane and J. Suryawanshi, Synthesis of samarium (Sm) doped thin film of SrMnO3 by pulse laser deposition and its structural and magnetic characterization. Current Science Perspectives, 1(2), 1-4 (2016).

[9] D. D. Dung, N. T. Hung and D. Odkhuu, Structure, optical and magnetic properties of new $Bi_{0.5}Na_{0.5}TiO_3$-$SrMnO_{3-\delta}$ solid solution materials. Scientific Reports, 9, 18186 (2019).

[10] S. Gholamrezaei, M. Salavati-Niasari, Sonochemical synthesis of SrMnO3 nanoparticles as an efficient and new catalyst for O2 evolution from water splitting reaction. Ultrasonics Sonochemistry, 40,651-663 (2018).

[11] C. Lu-Gang, L. Fa-Min, Z. Wen-Wu, Z. Dian, The Electronic Structures and Optical Properties of Substituted Rare-Earth Manganite $Tb_{1-x}Yb_xMnO_3$. Chin. Phys. Lett, 30 No.5, 053601-4 (2013).

[12] D. Risold, B. Hallsted., and L. J. Gauckler, The strontium-oxygen system. Calphad, 20(3), 353-361(1996).

[13] Y.Q. Gao, W. Wang, On the activation energy of crystallization in metallic glasses. J. Non-Cryst. Solids, 81, 129-134 (1986).

[14] S. A. Khalate, R. S. Kate, H. M. Pathan, R. J. Deokate, Structural and electrochemical properties of spray deposited molybdenum trioxide (α-MoO_3) thin films. J. Solid State Electrochem, 21, 2737–2746 (2017).

[15] S. K. Loyalka, C. A. Riggs, Inverse problem in diffuse reflectance spectroscopy: Accuracy of the Kubelka-Munk equations. Applied spectroscopy, 49(8) 1107-1110(1995).

[16] Y. A. Taya, H. M. Ali, E. Kh. Shokr, M. M. Abd El-Raheem, M.F. Hasaneen, Sh.A. Elkot, A. M. Hassan, A.M. Abdel Hakeem, Mn-doped molybdenum trioxide for photocatalysis and solar cell applications. Optical Materials, 121, 111614 (2021).

[17] J. Tauc, Amorphous and Liquid Semiconductors, Plenum, New York, page 37 (1974).

[18] R. Ghanem, W. Hzez, R. M'nassri, H. Rahmouni, M. Gassoumi, K. Khirouni, and S. Alaya, Structural, optical and electrical studies on Mn substituted $La_{0.6}Ga_{0.4}FeO_3$. Journal of Alloys and Compounds, 791,822-832 (2019).

[19] Mark Fox, Optical properties of solids, OXFORD University press, page 25 (2001).

[20] H. M. Ali, E. Kh. Shokr, A. V. Marchenko, Some optical and dielectric properties of spray deposited tin oxide thin films. Optoelectronics and Advanced Materials–Rapid Communications,7, 207-213 (2013).

[21] M. Rusop, K. Uma, T. Soga, T. Jimbo, Post-growth annealing of zinc oxide thin films pulsed laser deposited under enhanced oxygen pressure on quartz and silicon substrates. Materials Science and Engineering B, 127, 150-153 (2006).

[22] M. Becker, H. Y. Fan, Optical Properties of Semiconductors. II. Infra-Red Transmission of Germanium. Phys. Rev., 76, 1530-1540 (1949).

[23] J. I. Pankove, Optical Processes in Semiconductors, Dover Publications, Inc., NY., page 138-147 (1971).

[24] I. A. Abdel-Latif, A. Hassen, C. Zybill, M. Abdel-Hafiez, S. Allam, Th. El-Sherbini, The influence of tilt angle on the CMR in $Sm_{0.6}Sr_{0.4}MnO_3$. Journal of Alloys and Compounds, 452, 245–248 (2008).

[25] N. Pandey and A. K. Thakur, Studies on structural and electrical properties of SrMnO3−δ prepared in oxidising medium. Advances in Applied Ceramics, 109, 83-90 (2010).

[26] S. F. Wang, H. Yang, T. Xian, X.Q. Liu, Size-controlled synthesis and photocatalytic properties of $YMnO_3$ nanoparticles. Catal. Commun., 12, 625−628 (2011).

[27] J. Turner., G. Sverdrup, M. K. Mann, P.C. Maness, B. Kroposki, M. Ghirardi, R. J. Evans, D. Blake, Renewable hydrogen production. Int. J. Energy Res., 32, 379–407 (2008).

[28] Z. Xia, and S. Chan, Feasibility study of hydrogen generation from sodium borohydride solution for micro fuel cell applications. J. Power Sources, 152, 46–49 (2005).